Spatial ALD of Al_2O_3 and ZnO using heavy water

Sami Kinnunen[1,2], Timo Sajavaara[1,2]

[1] *Accelerator Laboratory, Department of Physics, University of Jyvaskyla, P. O. Box 35, FI-40014 University of Jyvaskyla, Finland*
[2] *Nanoscience Center, Department of Physics, University of Jyvaskyla, P. O. Box 35, FI-40014 University of Jyvaskyla, Finland*

Abstract

Al_2O_3 and ZnO thin films were deposited from trimethylaluminium (TMA) and diethylzinc (DEZ) in combination with water using cylindrical rotating substrate spatial atomic layer deposition (SALD). The depositions were done between 67 and 140 °C. The growth per cycle for Al_2O_3 varied between 0.75 and 2.0×10^{15}at./cm^2 per cycle and for ZnO between 0.52 and 1.07×10^{15}at./cm^2 per cycle. The hydrogen incorporation was studied by varying the deposition temperature and substrate rotation speed. The rotation speed affects the precursor exposure time (46–458 ms) and inert gas purging time (111–1120 ms). The results show that Al_2O_3 films can contain up to 25 at.% of hydrogen when the deposition temperature is 67 °C or the deposition exposure/purging times are short. The deposition of ZnO in similar conditions produces films with hydrogen concentrations up to 15 at.%. The source of impurity hydrogen was investigated by using heavy water, ^2H_2O, as an oxygen source. The main hydrogen isotope in the Al_2O_3 films at low temperatures and fast deposition speed was found to be ^{1}H, while at higher temperatures and lower deposition speeds ^{2}H isotope was dominant. For ZnO, ^{1}H was the majority hydrogen isotope in the films in all the studied deposition conditions except at the lowest rotation speed.

Keywords: `SALD, Al2O3, ZnO, ToF-ERDA, Heavy water`

1. Introduction

Conventional pulsed atomic layer deposition (ALD) consists of two or more precursor pulses separated in time with inert gas purging in between. Atomic layer deposition is a widely studied and used method to deposit pinhole free films with sub-nanometer thickness control, and it enables precise deposition on complex 3D-structures and high-aspect-ratio substrates [1–3]. While the conventional ALD can be considered as a temporal ALD, spatial atomic layer deposition (SALD) separates the precursor pulses in space rather than in time. This enables faster deposition, for example, for solar cell passivation [4–7] and the construction of roll-to-roll (R2R) reactors for flexible substrates [8, 9]. Fast large area deposition is also desired, for example, on packaging materials [10, 11], on organic electronics like memristors [12] or on organic light emitting diode (OLED) displays where thin and transparent gas and moisture permeation barriers are required [9, 10, 13, 14]. Spatial ALD also enables completely new substrates such as large area fabrics to be coated effectively with ALD [15]. Spatial ALD has great potential also in Li-ion battery [16–18] applications and printed electronics [19].

Temporal ALD is often performed at low pressure conditions enabling efficient gas transfer and purging of the by-products [2], while SALD can be operated even at atmospheric pressure [20, 21]. This can further increase the throughput since there is no need for pumping down to a low deposition pressure. With SALD the coating head is in close proximity to the substrate so that air cannot infiltrate to the reaction space between the coating head and substrate surface. Therefore, the deposition space and all the unreacted precursor molecules can be pumped without escaping. This removes the requirement for vacuum in the reactor space, making deposition with roll to roll and on large surface area substrates much more attractive.

The benefit of SALD is often believed to be that long purging times between the precursor pulses are not needed [22]. With temporal ALD at low deposition temperatures the purging times can be rather minutes than seconds [23, 24].

The close proximity of precursor head to substrate significantly decreases the adsorption of precursor molecules on reactor walls, present in the temporal ALD. Therefore, much shorter purging time is required, and high speed SALD has realised deposition rates as high as 1 nm/s [25, 26]. However, the picture is more complicated when the deposition temperature is low and the reaction and by-product desorption rates are slow. Understanding the non-ideal ALD-conditions is important especially when flexible organic substrates are used. These often start to deteriorate at higher temperatures required for the deposition of high quality thin films.

On the downside, spatial ALD does not enable easy and independent control of purging and precursor exposure time, characteristic to temporal ALD. As the precursor inlets inject the precursors continuously, also the consumption of precursors require optimisation in order to minimise the waste of the often expensive precursors [27]. In SALD, either the substrate is moved at constant speed in close proximity to the precursor inlets or regions, or the coating head containing the exposure/purge sequence is moved while the substrate remains stationary [28]. Therefore, the whole reactor configuration must be changed if the precursor exposure and purging time ratio is tuned. In order to address this challenge Yersak *et al.* used modular SALD-reactor where varying the exposure/purge ratio was realised through removable spacers[18]. However, in most cases with SALD it is possible to play only with purging and precursor flows and the control of process parameters is usually more limited compared to the temporal ALD.

ALD thin films deposited at low temperatures often contain significant amounts of hydrogen and other impurities originating from the precursors [23, 24, 29–33]. In this study we used heavy water, ^2H_2O, instead of normal water in two common ALD processes: Al_2O_3 from trimethylaluminium (TMA) and water, and ZnO from diethylzinc (DEZ) and water. ALD Al_2O_3 is an amorphous dielectric and can be used as a high-k layer in several applications, but it also has been studied as a moisture barrier for OLEDs and packaging [10, 13, 34]. ALD ZnO is a polycrystalline wide band gap semiconductor with wurtzite crystal struc-

ture [30, 35]. The electrical properties of ZnO are tunable through doping and, for example, aluminium doped ZnO (AZO) have been studied as a transparent conducting oxide [36]. In addition, Al_2O_3/ZnO nanolaminates are studied as barrier layers [37] as well as in biosensing applications due to their tunable optical properties [38–41].

Earlier we studied these two processes using heavy water with temporal ALD [24, 33] and we found out that, in addition to the deposition temperature, the purging time has a significant effect on impurity incorporation. Precursors containing rare isotopes have been used to study reaction mechanisms of the temporal ALD [29, 31, 42, 43] but to our knowledge this is the first time isotopic precursors are used to study SALD films. By varying the temperature and substrate velocity (precursor exposure/purge time) we found out that hydrogen/deuterium incorporation follows mostly similar trend as the deposition with temporal ALD in our previous studies [24, 33]. However, the temperature in which the majority hydrogen isotope shifts from ^{1}H to ^{2}H was found to be higher than with temporal ALD. We also found out that the growth-per-cycle (GPC) of the ZnO decreases more with increasing substrate rotation speed compared to Al_2O_3.

2. Experimental methods

A modified spatial ALD reactor, Beneq TFS 200R (Fig. 1), was used to deposit Al_2O_3 and ZnO films on a flexible Ti-coated polyethylene terephthalate (PET) (Rowo Coatings). Trimethylaluminium (Strem Chemicals, min. 98 %) and diethylzinc (Volatec, min. 99 %) were used as metal precursors and both normal (^1H_2O) and heavy water (^2H_2O, Medical Isotopes Inc., Pelham, NH, USA, 99.9 %) were used as oxygen precursors. Nitrogen (Linde AG, 99.999 % purity) was used as carrier gas and purging gas. All precursors were heated to 35 °C in order to increase their vapour pressure. The substrate was attached to a cylinder with a diameter of 10 cm and there is a 500 μm gap between the precursor nozzle and the substrate. During the deposition the cylinder is

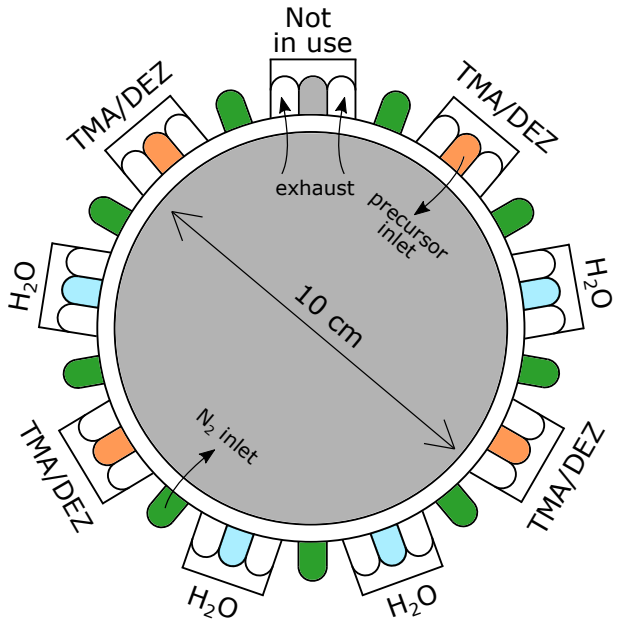

Figure 1: Schematics of the modified SALD reactor used in the study.

rotated so that the substrate passes through stationary precursor and purging zones. The reactor consisted of 4 TMA/DEZ and 4 water inlets divided by N_2 barrier flows. Due to the modification of the reactor, one rotation of the substrate cylinder effectively consists only of three ALD cycles as two of the TMA/DEZ and two of the H_2O inlets are successively as seen in Fig. 1. All Al_2O_3 samples and ZnO samples deposited using normal water were grown with 333 rotations. Due to the lower GPC, ZnO samples grown with heavy water were deposited with 500 rotations. Total nitrogen barrier flow during the deposition was 4600 sccm and both metal precursor and water were delivered using N_2 carrier gas flow of 100 sccm. During the deposition the base pressure in the reactor was 17–23 mbar depending on the deposition temperature.

Temperature series was carried out for both materials at deposition temperatures between 67 °C and 140 °C with substrate rotation speed of 10 rpm. In addition, the rotation speed e.g. the precursor exposure/purge time was varied by changing the substrate rotation speed between 5 and 50 rpm at the

deposition temperature of 100 °C.

The elemental compositions and film thicknesses were measured with time-of-flight elastic recoil detection analysis (ToF-ERDA) [44] using 13.615 MeV $^{63}Cu^{6+}$ incident ions for the Al_2O_3 samples and 13.615 MeV $^{127}I^{7+}$ for the ZnO samples. Elemental depth profiles were analysed with Potku software [45]. All the samples deposited with ^2H_2O were measured immediately after the deposition. This was done to ensure that the ^2H concentration does not change due to hydrogen exchange reactions with ambient moisture or hydrogen gas [24, 33].

3. Results and Discussion

The thicknesses and the elemental composition of the films were determined by means of ToF-ERDA depth profiles. In a ToF-ERDA measurement incident ions are accelerated in the energy range from few MeV to a few tens of MeVs towards the sample. Incident beam recoils sample atoms through elastic collisions towards a detector, in which the velocity (ToF) and the energy of these recoils are measured in coincidence. From ToF-energy histogram (Fig. 2a) different masses can be separated. This enables differentiating not only the elements but also the isotopes if there are no overlapping masses. The stopping power e.g. the energy loss of ions in medium as well as the scattering cross sections are well known. Therefore, quantitative elemental composition and a depth profile can be calculated without any reference samples. [44, 46]

The determination of absolute values for film thicknesses suffers from the substrate roughness and multiple scattering effects in ion beam analysis, especially with ZnO oxide films [47]. However, the relative trends in GPC can be observed and analysed. All the films (apart from Al_2O_3 films deposited at 67 °C with ^1H_2O) were conformal by visual inspection. In addition, depositing Al_2O_3 at 67 °C with ^2H_2O did not produce a proper film at all with the rotation speed of 10 rpm.

As an example, Fig. 2a presents the coincidence time-of-flight and energy histogram of a Al_2O_3 film deposited with TMA and ^2H_2O at 100 °C using 5 rpm

rotation speed. In Fig. 2b is shown a depth profile of the same sample. The elemental composition of all the samples is determined from the center of the film excluding both surface and interface regions.

The growth-per-cycle for Al_2O_3 films deposited with normal water is relatively independent on the deposition temperature between 85 and 140 °C when normal water is used, as seen in (Fig. 3a) and it is in line with our previous study with the temporal ALD [24]. However, the GPC is somewhat lower than often reported in the literature [23, 29, 48]. Ion beam techniques can measure the thicknesses in atoms/cm^2 rather than in nanometers. The thickness of 1×10^{15} at./cm^2 corresponds roughly to 1 Å if the density of Al_2O_3 is assumed to be the bulk value of 3.5 g/cm^3. However, it must be noted that ALD films deposited at low temperatures tend to be less dense than their bulk counterparts or even the ones deposited at higher temperatures [23]. Figure 3a shows also that the use of heavy water decreases the GPC slightly. This is most probably due to the kinetic isotope effect (KIE) which lowers the reaction rate by increasing the activation energy [49]. Similar effect has been detected for the temporal ALD [24, 33, 50]. It has also been previously shown with temporal ALD that water has a temperature dependent sticking probability and therefore the water pulse is the limiting factor at low temperatures [51, 52]. The lower GPC, when heavy water is used, is further evidence of water being the growth limiting precursor.

When the deposition temperature of Al_2O_3 was decreased to 67 °C the GPC increased rapidly due to the CVD-like growth. This is attributed in most studies to the adsorption of multiple layers of water at low deposition temperatures [23, 53, 54]. This will lead to excess water on the substrate surface which will in turn react with the next precursor leading to a more CVD-like growth if the purging time is not long enough for water to desorb. Maydannik *et al.* studied anomalous growth of SALD Al_2O_3 with similar reactor design as ours. They first suspected that mixing of the precursors is due to a boundary layer formed above the rotating substrate and this caused the high GPC [55]. Later they concluded that the higher than expected GPC can not be due to the

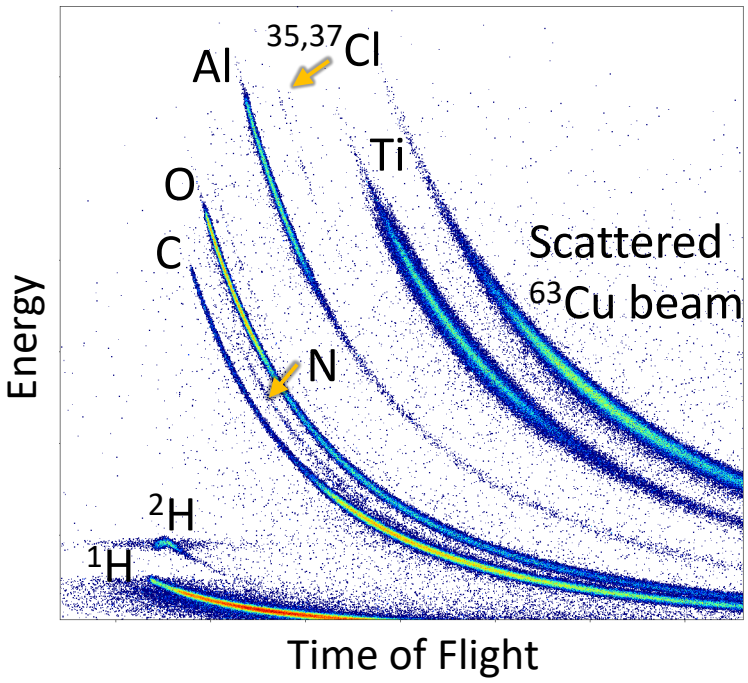

(a)

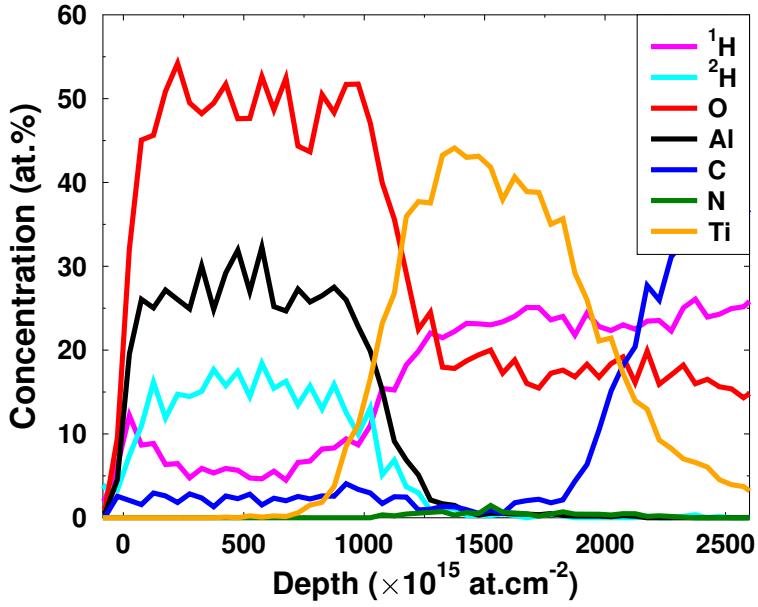

(b)

Figure 2: a) Coincidence time-of-flight and energy histogram of Al_2O_3 film deposited with TMA and ^2H_2O at 100 °C with 5 rpm. The film contains trace Cl at the surface and interface but it is omitted from the analysis for clarity. Minor amount of nitrogen from the Ti layer is also visible. b) Depth profile of the same sample where Ti film on top of PET substrate can be seen.

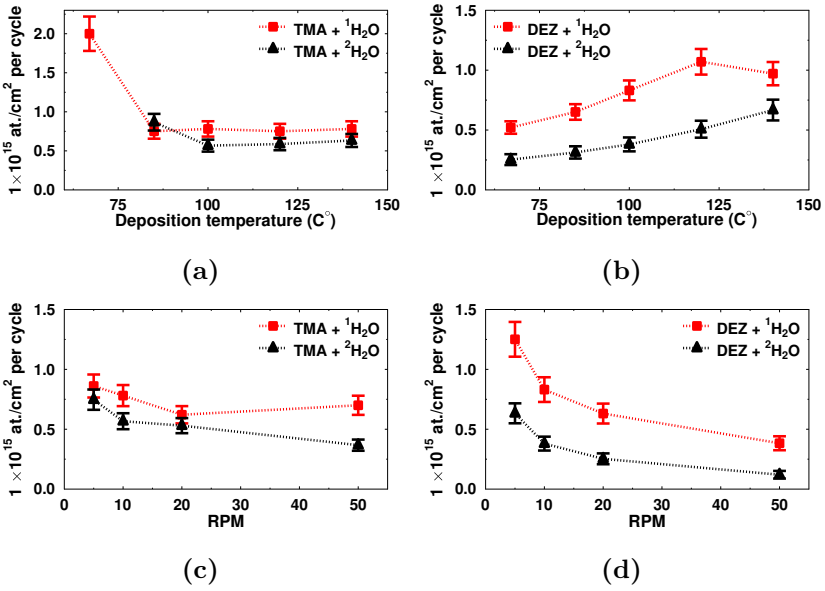

Figure 3: Growth per cycle determined from the ToF-ERDA depth profiles. GPC of a) Al_2O_3 and b) ZnO as a function of deposition temperature. The sample rotation speed was held at 10 rpm for all the samples. The GPC as a function of the substrate rotation speed at 100 °C for c) Al_2O_3 and d) ZnO.

boundary layer but must be due to the adsorpted excess water and insufficient purging at low deposition temperature [53]. Even though the CVD-growth can be a problem as shown above, the deposition of Al_2O_3 has been successfully demonstrated even near room temperature by both temporal [23] and spatial [48] ALD.

Interestingly, the excess growth does not seem to apply to DEZ + H_2O process. As seen in Fig. 3b, the anomalous CVD-growth is not observed even at 67 °C. The same observation was done in our previous article with temporal ALD [33]. In that study we could not find CVD-growth neither at low temperature (40 °C) nor with very short purging times (3 s) at 60 °C, both of which should lead to more than a monolayer of water based on the conclusions drawn from the Al_2O_3 depositions [24]. As DEZ is highly reactive towards water, it should also react with the excess water if it is available. Therefore, there are two possible intuitive explanations: 1) Adsorption of excess TMA contributes to the CVD-like growth which is absent with DEZ due to its faster desorption or 2) it is also possible, that the desorption rate of the excess water molecules on ZnO surface is much higher than on the Al_2O_3 surface and therefore CVD-growth is not detected on the ZnO surface.

The effect of heavy water on ZnO GPC is similar to Al_2O_3 but somewhat greater. No CVD-growth was detected even at low temperatures with heavy water, as seen in Fig. 3b. The GPC of the ZnO films seems also to be somewhat lower compared to reported values from temporal ALD studies [30, 33, 56, 57]. Low values of GPC for ZnO deposited with SALD around 100 °C compared to temporal ALD have also been reported by others [26, 35, 58]. In the case of ZnO, 1×10^{15} at./cm^2 corresponds to 1.2 Å if the bulk density 5.6 g/cm^3 is used. However, also ZnO films deposited at low temperature probably have lower density [57, 59] and therefore the GPC in Å/cycle is higher than expected from the bulk density. The GPC of ZnO increases with temperature which is also in line with temporal ALD. With ^1H_2O, the GPC starts to decrease at temperatures higher than 120 °C. The decrease in GPC at high deposition temperatures is characteristic to DEZ + H_2O process as the desorption of the OH-groups and

Table 1: Precursor residence and purge times with different substrate rotation speeds for each individual precursor nozzle and inert gas purging.

RPM	Residence time (ms)	Purge time (ms)
5	458	1120
10	229	559
20	115	280
50	46	111

physisorpted DEZ starts to limit the GPC [51, 60], although the maximum GPC is often observed around 150 °C [33, 56, 57, 61]. The temperature where the maximum GPC is achieved can depend on the process parameters as demonstrated by Nelson *et al.* [62]. They showed that the temperature of maximum GPC of SALD ZnO films depend on the pulse/purge time.

Both Al_2O_3 and ZnO films were deposited at 100 °C with varying rotation speed. In our previous work [24] we found out that the purging time did not change the GPC of TMA + H_2O deposition at 100 °C when all the other parameters were kept constant. From Fig. 3c can be concluded that the rotation speed has an effect on the GPC of Al_2O_3, but the reduction with increased rotation speed is much more pronounced with ZnO as seen in Fig. 3d. There is earlier evidence of DEZ soft saturation [18, 19, 62–64] and the increase in GPC towards slower speed could be because of the longer precursor exposure time. However, in our study with temporal ALD we showed that just by increasing the purging times increased the GPC of ZnO deposition at 60 °C [33]. Therefore, in the case of ZnO, it is possible that the increasing GPC at slower substrate rotation speeds is not only due to the increasing exposure time but also a result of longer purging. On the other hand, at higher deposition temperatures than used in this study, increasing the purging time has been found to decrease the GPC due to desorption of reaction sites [62, 65]. The precursor exposure and purging times with different rotation speeds are shown in Table 1. However, due to the modification of the reactor (Fig. 1), there is one TMA/DEZ and one H_2O

double pulse in every rotation. The rotation speed of 10 rpm used in temperature series with exposure time of 229 ms should be more than sufficient. While the precursor exposure times vary significantly from study to study, exposure times of even as short as 8 ms have been reported for ZnO [58]. However, exposure times in range of few tens of milliseconds are often reported for SALD processes [19, 25, 26, 36, 62, 66].

In our previous study we found signs of transient steric hindrance when depositing ZnO [33] proposed by [67]. In our study we separated the precursor pulses into three shorter pulses at 40 °C while keeping the precursor exposure unchanged. This increased the GPC by 33 %. This transient steric hindrance can be due to the slow reactions and slowly desorbing by-products that block the reaction sites temporarily. Similar approach was also utilised by Muneshwar and Cadien [68] and they found that bulkier ligands emphasise the effect. As ethyl-ligands in DEZ are bulkier than methyls in TMA, the effect should be more pronounced with the ZnO process and this is supported by the experiment. Therefore, it is possible that the reaction rate and the desorption of by-products can inhibit the growth of ZnO if the purging is too short. It is also possible that the soft-saturation of ZnO is not a separate phenomenon but just a consequence of the transient steric hindrance.

The elemental composition of the films was determined with ToF-ERDA and all the results are presented in Tables 2–5. The stoichiometry of the main components of the films changes considerably with both the deposition temperature (Figs. 4a and 4b) and rotation speed (Figs. 4c and 4d). Both Al_2O_3 and ZnO films were oxygen rich which seems to be typical for low temperature deposition of these processes [23, 24, 29, 30, 33, 69]. Increasing both the temperature and the exposure/purge time improves the film quality and produces films closer to the stoichiometric O/Al ratio (1.5) and O/Zn ratio (1). Again, the films deposited with heavy water tend to be somewhat less optimal due to the lower reactivity of ^2H_2O. Especially ZnO deposited with high substrate velocity and heavy water is very far from stoichiometric ZnO. Measuring the O/Zn ratio with ToF-ERDA using ^{127}I ion beam suffers from the multiple scattering and as a

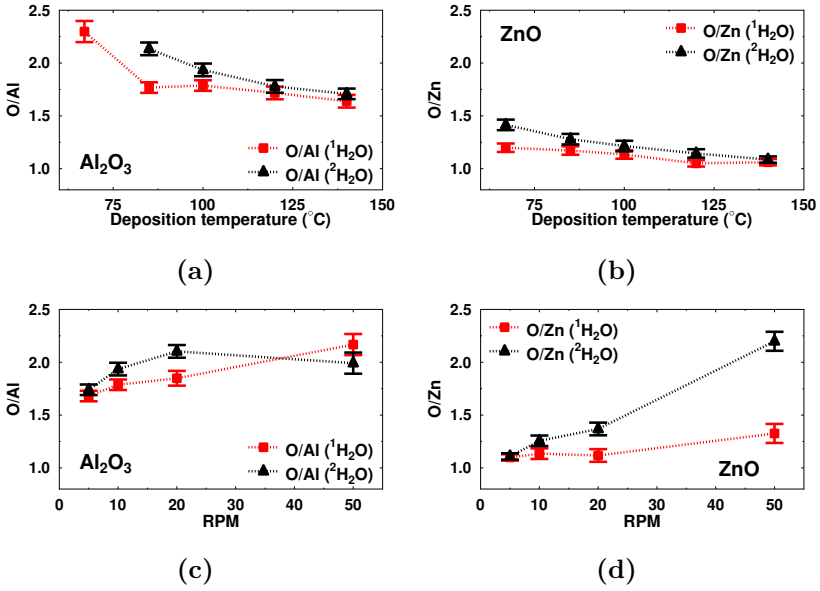

Figure 4: Ratio of a) O/Al and b) O/Zn as a function of the deposition temperature. The rotation speed was kept at 10 rpm. Ratio of c) O/Al and d) O/Zn as a function of the rotation speed. The deposition temperature was kept at 100 °C.

result the concentration of Zn is somewhat underestimated [47]. However, the results presented in Figs. 4b and 4d show that the O/Zn ratio approaches the ideal ratio of 1 as the temperature is increased or the rotation speed is slowed. The high oxygen concentration for both Al_2O_3 and ZnO at low temperatures would imply that many unreacted OH-groups are buried in the film leading to higher than expected oxygen concentration. The hydrogen concentrations in these films point towards the same explanation.

The hydrogen impurities in the Al_2O_3 and ZnO films can originate from two sources: 1) From the metal precursor, TMA or DEZ, which both contain alkyl groups or 2) from unreacted OH-groups originating from water. The simplified reaction mechanism of TMA/DEZ with water leading to methane/ethane by-products has been somewhat challenged in recent years. Gurre-Nuñez *et al.* found a relation between the high O/Al ratio and deuterium concentration [29] in Al_2O_3 films deposited with temporal ALD. They concluded that most of the hydrogen, in the form of deuterium, is left in the films due rehydroxylation of oxygen atoms in subsequent cycles. On the other hand, there are evidence of persistent methyl-groups in the case of Al_2O_3 [43, 51] that do not react with water at low deposition temperatures even with excessive pulsing of water. Sperling *et al.* concluded that the presence of persistent CH_3 is due to the coverage dependent activation energy [70]. Towards the end of the water pulse, when CH_3 coverage is low, the reaction barrier increases making the reaction of isolated CH_3-groups unlikely. These groups could get buried in the film in subsequent pulses. However, the films have often very low carbon concentration [24, 29, 30, 33, 43] which implies that these persistent groups are not incorporated into the film. Persistent methyl groups probably react with water in subsequent cycles but definitive explanation is not yet given. In addition, Werbrouck *et al.* [71] found out that there is potentially a secondary reaction pathway causing etching of the already reacted species during the H_2O pulse. Similarly to TMA-process, persistent ethyl ligands have been observed to stay unreacted at the surface of the ZnO films deposited from DEZ and water at low deposition temperatures. These persistent ethyls have been both experimentally

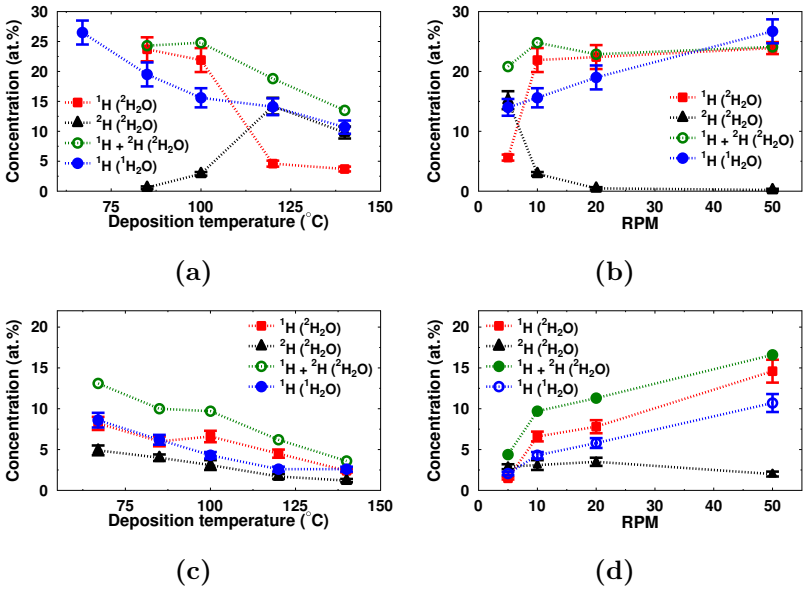

Figure 5: ^{1}H and ^{2}H concentrations of the films as a function of the deposition temperature for a) Al_2O_3 and b) ZnO. The substrate rotation speed was kept at 10 rpm. ^{1}H and ^{2}H concentrations of the films as a function of the rotation speed deposited at 100 °C for c) Al_2O_3 and d) ZnO.

observed [72] and computationally predicted [60].

The hydrogen concentration of the Al_2O_3 and ZnO deposited with ^1H_2O process follows an expected trend of decreasing concentration with increasing deposition temperature, reported in many studies before with temporal ALD for both Al_2O_3 [23, 24, 29, 51] and ZnO [30, 31, 33] as seen in Figs. 5a and 5c. Compared to temporal ALD, the hydrogen concentration of SALD films is somewhat higher.

When heavy water is used, the total hydrogen and deuterium concentrations are slightly higher than with the normal water, which is in agreement with isotopic effect discussed earlier. These results are also in agreement with previous work with temporal ALD [24, 33]. In the case of Al_2O_3 with heavy water, we see a change in majority hydrogen isotope (Fig. 5a) similar to our previous work with Al_2O_3 films deposited with temporal ALD [24]. As the deposition

Table 2: The elemental composition of Al_2O_3 films deposited at different temperatures with both normal (^1H_2O) and heavy water (^2H_2O).

	T (°C)	Al	O	C	^{1}H	^{2}H	tot H	GPC (1×10^{15} at/cm^2)	Deposition rate (1×10^{15}at/cm^2 per s)
^1H_2O	67	22	50	1.7	26.5	-	26.5	2.0	1.0
	85	28	50	3	19.5	-	19.5	0.75	0.38
	100	30	53	1.9	15.6	-	15.6	0.78	0.39
	120	30	52	3.3	14.1	-	14.1	0.75	0.38
	140	33	54	1.6	10.7	-	10.7	0.78	0.39
^2H_2O	67	-	-	-	-	-	-	-	-
	85	24	51	1.1	23.7	0.6	24.3	0.87	0.43
	100	25	48	2.7	21.9	2.9	24.8	0.57	0.28
	120	29	51	1.9	4.6	14.2	18.8	0.59	0.29
	140	31	53	1.9	3.7	9.8	13.5	0.63	0.32

temperature is decreased below 120 °C, the main hydrogen source changes from deuterium to hydrogen. With temporal ALD the same shift was observed between 70 and 80 °C. In addition to the temperature, this phenomenon is related to the purging times, which can explain the difference in the temperature. With temporal ALD, a similar change of the main impurity isotope was observed also at 100 °C, when purging times were decreased to 3 s. This can be due to the slowly reacting CH_3-groups discussed earlier, some of which do not react with water even with very long precursor exposure and purging times [51] if the deposition temperature is low. With too short reaction and purging times there might not be enough time to remove these methyl groups and many of them are buried in the film. Increasing the temperature increases the energy available for the reaction to overcome the barrier and more and more of these methyl groups react leaving less ^{1}H in the film.

As mentioned above, the effect of the purging time to majority hydrogen isotope concentration is evident when the rotation speed is varied as seen in Fig 5b. With 5 rpm (longest exposure/purge) the main hydrogen isotope is ^{2}H, but as the rotation speed is increased and the time for the reaction to go to the completion is too short, the main hydrogen isotope changes to ^{1}H. This effect of changing majority hydrogen isotopes is visible when short purging times are

Table 3: The elemental composition of ZnO films deposited at different temperatures with both normal (^1H_2O) and heavy water (^2H_2O).

	T (°C)	Zn	O	C	^{1}H	^{2}H	tot H	GPC (1×10^{15} at/cm^2)	Deposition rate (1×10^{15}at/cm^2 per s)
^1H_2O	67	41	50	0.7	8.6	-	8.6	0.52	0.26
	85	43	50	0.4	6.2	-	6.2	0.65	0.33
	100	45	51	0.4	4.3	-	4.3	0.83	0.42
	120	47	50	0.3	2.6	-	2.6	1.07	0.54
	140	47	50	0.4	2.6	-	2.6	0.97	0.49
^2H_2O	67	37	49	0.7	8.2	4.9	13.1	0.25	0.13
	85	39	50	0.9	6	4	10.0	0.31	0.16
	100	39	49	1.5	6.6	3.1	9.7	0.38	0.19
	120	43	49	1.8	4.5	1.7	6.2	0.51	0.25
	140	45	50	1.1	2.4	1.2	3.6	0.67	0.33

used in temporal ALD, so it is not related only to the too short exposure times in itself. The results with SALD are in good agreement with our previous studies with temporal ALD [24, 33] where we showed that purging time has a big effect on hydrogen/deuterium incorporation even though the GPC does not change significantly.

With temporal ALD, a similar change of the majority hydrogen isotope incorporation was found also for the DEZ+^2H_2O process [33]. However, in our SALD process, ^{1}H remained as the main hydrogen isotope regardless of the deposition temperature (Fig. 5c). A likely explanation for the high ^{1}H concentration is too fast rotation speed (10 rpm) for the given temperature (100 °C). This conclusion is supported by the change of the GPC in Fig. 3d, as the GPC was found to increase significantly as the rotation speed was decreased to 5 rpm at 100 °C. More evidence of this is the hydrogen/deuterium concentration when rotation speed of 5 rpm is used (Fig. 5d). As the rotation speed is decreased to 5 rpm, the ^{1}H concentration goes just below the ^{2}H concentration, similar to when long purging times are used in temporal ALD [33].

The high oxygen concentration at low deposition temperatures does not seem to lead to a high deuterium concentration as would be expected if the excess oxygen is in the form of buried O^{2}H-groups suggested by Guerra-Nuñez

Table 4: The elemental composition of Al_2O_3 films deposited at with different rotation speeds at 100 °C with both normal (^1H_2O) and heavy water ^2H_2O.

	RPM	Al	O	C	^{1}H	^{2}H	tot H	GPC (1×10^{15} at/cm^2)	Deposition rate (1×10^{15}at/cm^2 per s)
^1H_2O	5	31	53	1.6	14.0	-	14.0	0.86	0.22
	10	30	53	1.9	15.6	-	15.6	0.78	0.39
	20	28	51	2.0	19.0	-	19.0	0.62	0.62
	50	23	49	1.4	27	-	27	0.70	1.75
^2H_2O	5	28	49	2.2	5.6	15.2	20.8	0.75	0.19
	10	25	48	2.7	21.9	2.9	24.8	0.57	0.28
	20	24	51	1.7	22.4	0.5	22.9	0.53	0.53
	50	24	48	2.9	23.9	0.2	24.1	0.37	0.92

et al. [29]. However, the situation is quite the opposite: the higher the ^{1}H concentration is the higher the O/Al and O/Zn ratios are. From the previous studies we know that both Al_2O_3 and ZnO films deposited with ALD have very low carbon concentration even at low deposition temperatures [24, 29, 30, 33, 43]. As seen in the Tables 2–5, the carbon concentration is not strongly dependent on the process parameters for Al_2O_3 and the carbon concentration was between 1.4 and 3.3 at.%. For the ZnO films the carbon concentration varied between 0.3 and 2.8 at.% and there is a clear dependency on rotation speed but the maximum concentration stays rather low. These numbers are low if we consider the ^{1}H concentration of the films deposited with low deposition temperature or fast rotation speeds. If the ^{1}H would originate purely from the embedded methyl/ethyl groups, the carbon concentration should be significantly higher. From previous studies [24, 33] we know that ^{2}H migrates within the film and can be replaced by ^{1}H from ambient gasses. This effect was minimized by measuring all the films containing ^{2}H immediately after the deposition exposing the film for ambient condition only for couple of minutes. However, it is not impossible that the ^{1}H/^{2}H exchange reactions take place already during the deposition leading to higher than expected ^{1}H concentration.

In our previous studies the higher ^{1}H concentration compared to the ^{2}H concentration was found to be related to too short purging times for the given

Table 5: The elemental composition of ZnO films deposited at with different rotation speeds at 100 °C with both normal (^1H_2O) and heavy water (^2H_2O).

	RPM	Zn	O	C	^{1}H	^{2}H	tot H	GPC (1×10^{15} at/cm^2)	Deposition rate (1×10^{15} at/cm^2 per s)
^1H_2O	5	47	51	0.3	2.1	-	2.1	1.25	0.31
	10	45	51	0.4	4.3	-	4.3	0.83	0.42
	20	44	49	0.6	5.8	-	5.8	0.63	0.63
	50	38	50	1.0	10.7	-	10.7	0.38	0.96
^2H_2O	5	45	50	0.3	1.5	2.9	4.4	0.63	0.16
	10	39	49	1.5	6.6	3.1	9.7	0.38	0.19
	20	37	51	1.2	7.8	3.5	11.3	0.25	0.25
	50	25	55	2.8	14.6	2.0	16.6	0.12	0.3

temperature. The films deposited at "ideal" conditions (high enough temperature, long purging times) had always higher ^{2}H concentration than ^{1}H concentration for both Al_2O_3 and ZnO. For example, Guerra-Nuñez *et al.* [29] and Guziewicz *et al.* [31] reported ^{2}H to be the majority hydrogen isotope at similar deposition temperatures in Al_2O_3 and ZnO films, respectively. Both of them used long purging times which explains why they did not found films with ^{1}H as a majority hydrogen isotope. However, results obtained by Hiraiwa *et al.* [50] on ^{1}H/^{2}H concentration of Al_2O_3 are somewhat mixed. Similar to us, they reported ^{1}H to be the majority isotope at 100 °C, and at higher temperature (450 °C) the ^{2}H concentration was higher than the ^{1}H concentration. However, they reported that the total hydrogen concentration at 450 °C was higher when normal water was used. In a recent study Xia *et al.* reported quite contradictory results on ZnO films [57] compared to our results in this and in our previous study [33]. According to them the ^{1}H concentration is higher than ^{2}H concentration in all deposition temperatures between 100 and 300 °C even though they have used long (60 s) purging times. This emphasises the need for precise description and consideration of the process parameters since they will impact the film composition and other properties, and the conclusions drawn from them. This question has earlier been addressed, for example, by Sønsteby *et al.* [73].

As seen from Tables 2–5, the actual deposition rate in 10^{15} at./cm^2/s increases with increasing substrate rotation speed even if the GPC decreases. This is true for both Al_2O_3 and ZnO but the GPC of ZnO decreases more rapidly with increasing rotation speed. Therefore, the actual increase in throughput of ZnO is significantly lower than with Al_2O_3. On the other hand, a high deposition speed also leads to lower quality films with higher impurity concentrations. This can, for example, have an effect on the electrical properties of the film [74, 75]. Also, the barrier properties of the film can be affected by the high impurity concentrations. For example, hydrogen incorporation impacts indirectly the performance of ALD films in moisture and gas barrier applications. Films with high hydrogen concentration are known to be less dense [23, 29, 76], leading often to a poor barrier quality when low deposition temperature or fast deposition speed is used [9, 13, 34]. However, the deposition rate achieved by the SALD at low temperatures can be an order of magnitude higher than with temporal ALD making it an attractive option if satisfactory film quality can be reached.

4. Conclusions

Both Al_2O_3 and ZnO films contain ^{1}H and ^{2}H when deposited with heavy water. The main hydrogen isotope in the films depends on the deposition conditions so that more ideal conditions (high temperature or long exposure/purge times) seem to favour incorporation of ^{2}H over ^{1}H. For low deposition temperature and short exposure/purge times the results are quite the opposite. This is in line with the results obtained from temporal ALD studies [24, 33]. After the deposition at non-ideal conditions both films are also highly oxygen rich. Deuterium gets incorporated presumably in the films as OH-groups, which should lead to high O and ^{2}H concentrations. On the other hand, high ^{1}H concentration does not lead to as high carbon concentration as would be expected if methyl/ethyl groups are buried into the films. These assumptions are in contradiction with each other. Our results show that the mechanism behind the

simultaneous high oxygen and ^{1}H concentrations at non-ideal deposition conditions is related to inadequate purging at given temperature, but requires further studies to be understood completely.

Deposition of thin films with spatial ALD requires precise consideration in order to produce high quality and low impurity films. The throughput i.e. the growth rate (Å/s) of the ALD deposition can be sped up considerably by shortening the exposure/purging time. Even though the growth-per-cycle decreases, the throughput can increase due to shorter cycle times. The throughput of the Al_2O_3 increases significantly with increasing rotation speed while the GPC of the ZnO suffers more from shorter exposure/purging times. However, the increase in throughput does not come without a cost and leads to higher impurity concentration. In addition, the precursor exposure and purge times can not be as easily or independently changed as in temporal ALD. This makes the design and construction of a SALD-reactor that is suitable for multitude of processes much more challenging.

References

[1] R. L. Puurunen, Surface chemistry of atomic layer deposition: A case study for the trimethylaluminum/water process, Journal of Applied Physics 97 (2005) 121301.

[2] S. M. George, Atomic Layer Deposition: An Overview, Chemical Reviews 110 (2010) 111–131. PMID: 19947596.

[3] V. Miikkulainen, M. Leskelä, M. Ritala, R. Puurunen, Crystallinity of inorganic films grown by atomic layer deposition: Overview and general trends, Journal of Applied Physics 113 (2013) 021301.

[4] P. Poodt, V. Tiba, F. Werner, J. Schmidt, A. Vermeer, F. Roozeboom, Ultrafast atomic layer deposition of alumina layers for solar cell passivation, Journal of The Electrochemical Society 158 (2011) H937.

[5] C. Frijters, P. Poodt, A. Illiberi, Atmospheric spatial atomic layer deposition of Zn(O,S) buffer layer for Cu(In,Ga)Se_2 solar cells, Solar Energy Materials and Solar Cells 155 (2016) 356–361.

[6] Z. Xing, J. Xiao, T. Hu, X. Meng, D. Li, X. Hu, Y. Chen, Atomic Layer Deposition of Metal Oxides in Perovskite Solar Cells: Present and Future, Small Methods (2020) 2000588.

[7] B. Vermang, A. Rothschild, A. Racz, J. John, J. Poortmans, R. Mertens, P. Poodt, V. Tiba, F. Roozeboom, Spatially separated atomic layer deposition of Al_2O_3, a new option for high-throughput Si solar cell passivation, Progress in Photovoltaics: Research and Applications 19 (2011) 733–739.

[8] D. Muñoz-Rojas, V. H. Nguyen, C. Masse de la Huerta, S. Aghazadehchors, C. Jiménez, D. Bellet, Spatial Atomic Layer Deposition (SALD), an emerging tool for energy materials. Application to new-generation photovoltaic devices and transparent conductive materials, Comptes Rendus Physique 18 (2017) 391 – 400. Demain l'énergie.

[9] P. S. Maydannik, T. O. Kääriäinen, K. Lahtinen, D. C. Cameron, M. Söderlund, P. Soininen, P. Johansson, J. Kuusipalo, L. Moro, X. Zeng, Roll-to-roll atomic layer deposition process for flexible electronics encapsulation applications, Journal of Vacuum Science & Technology A 32 (2014) 051603.

[10] T. O. Kääriäinen, P. Maydannik, D. C. Cameron, K. Lahtinen, P. Johansson, J. Kuusipalo, Atomic layer deposition on polymer based flexible packaging materials: Growth characteristics and diffusion barrier properties, Thin Solid Films 519 (2011) 3146–3154.

[11] K. Lahtinen, T. Kääriäinen, P. Johansson, S. Kotkamo, P. Maydannik, T. Seppänen, J. Kuusipalo, D. C. Cameron, UV protective zinc oxide coating for biaxially oriented polypropylene packaging film by atomic layer deposition, Thin Solid Films 570 (2014) 33–37.

[12] K. Ali, J. Ali, S. M. Mehdi, K.-H. Choi, Y. J. An, Rapid fabrication of Al_2O_3 encapsulations for organic electronic devices, Applied Surface Science 353 (2015) 1186–1194.

[13] K. L. Jarvis, P. J. Evans, Growth of thin barrier films on flexible polymer substrates by atomic layer deposition, Thin Solid Films 624 (2017) 111–135.

[14] M. Aghaee, P. S. Maydannik, P. Johansson, J. Kuusipalo, M. Creatore, T. Homola, D. C. Cameron, Low temperature temporal and spatial atomic layer deposition of TiO_2 films, Journal of Vacuum Science & Technology A 33 (2015) 041512.

[15] M. B. M. Mousa, J. S. Ovental, A. H. Brozena, C. J. Oldham, G. N. Parsons, Modeling and experimental demonstration of high-throughput flow-through spatial atomic layer deposition of Al_2O_3 coatings on textiles at atmospheric pressure, Journal of Vacuum Science & Technology A 36 (2018) 031517.

[16] C.-H. Chao, C.-T. Hsieh, W.-J. Ke, L.-W. Lee, Y.-F. Lin, H.-W. Liu, S. Gu, C.-C. Fu, R.-S. Juang, B. C. Mallick, Y. A. Gandomi, C.-Y. Su, Roll-to-roll atomic layer deposition of titania coating on polymeric separators for lithium ion batteries, Journal of Power Sources 482 (2021) 228896.

[17] S. Moitzheim, J. E. Balder, P. Poodt, S. Unnikrishnan, S. De Gendt, P. M. Vereecken, Chlorine Doping of Amorphous TiO_2 for Increased Capacity and Faster Li^+-Ion Storage, Chemistry of Materials 29 (2017) 10007–10018.

[18] A. S. Yersak, K. Sharma, J. M. Wallas, A. A. Dameron, X. Li, Y. Yang, K. E. Hurst, C. Ban, R. C. Tenent, S. M. George, Spatial atomic layer deposition for coating flexible porous Li-ion battery electrodes, Journal of Vacuum Science & Technology A 36 (2018) 01A123.

[19] C. R. Ellinger, S. F. Nelson, Selective Area Spatial Atomic Layer Deposition of ZnO, Al_2O_3, and Aluminum-Doped ZnO Using Poly(vinyl pyrrolidone), Chemistry of Materials 26 (2014) 1514–1522.

[20] D. Muñoz-Rojas, T. Maindron, A. Esteve, F. Piallat, J. Kools, J.-M. Decams, Speeding up the unique assets of atomic layer deposition, Materials Today Chemistry 12 (2019) 96–120.

[21] K. P. Musselman, C. F. Uzoma, M. S. Miller, Nanomanufacturing: High-throughput, cost-effective deposition of atomic scale thin films via atmospheric pressure spatial atomic layer deposition, Chemistry of Materials 28 (2016) 8443–8452.

[22] P. Poodt, D. C. Cameron, E. Dickey, S. M. George, V. Kuznetsov, G. N. Parsons, F. Roozeboom, G. Sundaram, A. Vermeer, Spatial atomic layer deposition: A route towards further industrialization of atomic layer deposition, Journal of Vacuum Science & Technology A 30 (2012) 010802.

[23] M. D. Groner, F. H. Fabreguette, J. W. Elam, S. M. George, Low-Temperature Al_2O_3 Atomic Layer Deposition, Chemistry of Materials 16 (2004) 639–645.

[24] S. Kinnunen, K. Arstila, T. Sajavaara, Al_2O_3 ALD films grown using TMA + rare isotope ${}^2H_2^{16}O$ and ${}^1H_2^{18}O$ precursors, Applied Surface Science (2021) 148909.

[25] P. Poodt, A. Lankhorst, F. Roozeboom, K. Spee, D. Maas, A. Vermeer, High-Speed Spatial Atomic-Layer Deposition of Aluminum Oxide Layers for Solar Cell Passivation, Advanced Materials 22 (2010) 3564–3567.

[26] A. Illiberi, F. Roozeboom, P. Poodt, Spatial Atomic Layer Deposition of Zinc Oxide Thin Films, ACS Applied Materials & Interfaces 4 (2012) 268–272. PMID: 22171693.

[27] V. H. Nguyen, A. Sekkat, C. Jiménez, D. Muñoz, D. Bellet, D. Muñoz-Rojas, Impact of precursor exposure on process efficiency and film properties in spatial atomic layer deposition, Chemical Engineering Journal 403 (2021) 126234.

[28] David Muñoz-Rojas, Viet Huong Nguyen, César Masse de la Huerta, Carmen Jiménez and Daniel Bellet, Spatial Atomic Layer Deposition, Chemical Vapor Deposition for Nanotechnology, IntechOpen, 2019. doi:10.5772/intechopen.82439.

[29] C. Guerra-Nuñez, M. Döbeli, J. Michler, I. Utke, Reaction and Growth Mechanisms in Al_2O_3 deposited via Atomic Layer Deposition: Elucidating the Hydrogen Source, Chemistry of Materials 29 (2017) 8690–8703.

[30] J. Malm, E. Sahramo, J. Perälä, T. Sajavaara, M. Karppinen, Low-temperature atomic layer deposition of ZnO thin films: Control of crystallinity and orientation, Thin Solid Films 519 (2011) 5319–5322.

[31] E. Guziewicz, W. Wozniak, S. Mishra, R. Jakiela, M. Guziewicz, V. Y. Ivanov, E. Lusakowska, R. Schifano, Hydrogen in As-Grown and Annealed ZnO Films Grown by Atomic Layer Deposition, physica status solidi (a) 218 (2021) 2000318.

[32] M. Napari, J. Malm, R. Lehto, J. Julin, K. Arstila, T. Sajavaara, M. Lahtinen, Nucleation and growth of ZnO on PMMA by low-temperature atomic layer deposition, Journal of Vacuum Science & Technology A 33 (2015) 01A128.

[33] S. Kinnunen, M. Lahtinen, K. Arstila, T. Sajavaara, Hydrogen and Deuterium Incorporation in ZnO Films Grown by Atomic Layer Deposition, Coatings 11 (2021).

[34] H. G. Kim, S. S. Kim, Aluminum oxide barrier coating on polyethersulfone substrate by atomic layer deposition for barrier property enhancement, Thin Solid Films 520 (2011) 481–485.

[35] M.-J. Zhao, Z.-T. Sun, C.-H. Hsu, P.-H. Huang, X.-Y. Zhang, W.-Y. Wu, P. Gao, Y. Qiu, S.-Y. Lien, W.-Z. Zhu, Zinc Oxide Films with High Transparency and Crystallinity Prepared by a Low Temperature Spatial Atomic Layer Deposition Process, Nanomaterials 10 (2020).

[36] D. B. Fullager, G. D. Boreman, C. D. Ellinger, T. Hofmann, Broadband optical properties of aluminium zinc oxide thin films prepared by spatial atomic layer deposition, Thin Solid Films 653 (2018) 267–273.

[37] D. won Choi, S.-J. Kim, J. H. Lee, K.-B. Chung, J.-S. Park, A study of thin film encapsulation on polymer substrate using low temperature hybrid ZnO/Al_2O_3 layers atomic layer deposition, Current Applied Physics 12 (2012) S19–S23. Proceedings of the Second International Symposium on Hybrid Materials and Processing Busan, Korea, 27-29 October 2011.

[38] A. A. Chaaya, R. Viter, I. Baleviciute, M. Bechelany, A. Ramanavicius, Z. Gertnere, D. Erts, V. Smyntyna, P. Miele, Tuning Optical Properties of Al_2O_3/ZnO Nanolaminates Synthesized by Atomic Layer Deposition, The Journal of Physical Chemistry C 118 (2014) 3811–3819.

[39] J. López, J. Martínez, N. Abundiz, D. Domínguez, E. Murillo, F. Castillón, R. Machorro, M. Farías, H. Tiznado, Thickness effect on the optical and morphological properties in Al_2O_3/ZnO nanolaminate thin films prepared by atomic layer deposition, Superlattices and Microstructures 90 (2016) 265–273.

[40] R. Viter, I. Iatsunskyi, V. Fedorenko, S. Tumenas, Z. Balevicius, A. Ramanavicius, S. Balme, M. Kempiński, G. Nowaczyk, S. Jurga, M. Bechelany, Enhancement of Electronic and Optical Properties of ZnO/Al_2O_3 Nanolaminate Coated Electrospun Nanofibers, The Journal of Physical Chemistry C 120 (2016) 5124–5132.

[41] Z. Balevicius, A. Paulauskas, I. Plikusiene, L. Mikoliunaite, M. Bechelany, A. Popov, A. Ramanavicius, A. Ramanaviciene, Towards the application of Al_2O_3/ZnO nanolaminates in immunosensors: total internal reflection spectroscopic ellipsometry based evaluation of BSA immobilization, J. Mater. Chem. C 6 (2018) 8778–8783.

[42] M. Juppo, A. Rahtu, M. Ritala, M. Leskelä, In situ mass spectrometry study on surface reactions in atomic layer deposition of Al_2O_3 thin films

from trimethylaluminum and water, Langmuir 16 (2000) 4034–4039. Cited By 94.

[43] V. Vandalon, W. M. M. E. Kessels, Revisiting the growth mechanism of atomic layer deposition of Al_2O_3: A vibrational sum-frequency generation study, Journal of Vacuum Science & Technology A 35 (2017) 05C313.

[44] M. Laitinen, M. Rossi, J. Julin, T. Sajavaara, Time-of-flight – Energy spectrometer for elemental depth profiling – Jyväskylä design, Nuclear Instruments and Methods in Physics Research Section B: Beam Interactions with Materials and Atoms 337 (2014) 55–61.

[45] K. Arstila, J. Julin, M. Laitinen, J. Aalto, T. Konu, S. Kärkkäinen, S. Rahkonen, M. Raunio, J. Itkonen, J.-P. Santanen, T. Tuovinen, T. Sajavaara, Potku – New analysis software for heavy ion elastic recoil detection analysis, Nuclear Instruments and Methods in Physics Research Section B: Beam Interactions with Materials and Atoms 331 (2014) 34 – 41. 11th European Conference on Accelerators in Applied Research and Technology.

[46] K. Yasuda, time-of-flight erda for depth profiling of light elements (????).

[47] K. Arstila, T. Sajavaara, J. Keinonen, Monte carlo simulation of multiple and plural scattering in elastic recoil detection, Nuclear Instruments and Methods in Physics Research Section B: Beam Interactions with Materials and Atoms 174 (2001) 163–172.

[48] K. Ali, K.-H. Choi, Low-Temperature Roll-to-Roll Atmospheric Atomic Layer Deposition of Al_2O_3 Thin Films, Langmuir 30 (2014) 14195–14203. PMID: 25407477.

[49] M. Gómez-Gallego, M. Sierra, Kinetic Isotope Effects in the Study of Organometallic Reaction Mechanisms, Chemical Reviews 111 (2011) 4857–4963. PMID: 21545118.

[50] A. Hiraiwa, T. Saito, D. Matsumura, H. Kawarada, Isotope analysis of diamond-surface passivation effect of high-temperature H_2O-grown atomic layer deposition-Al_2O_3 films, Journal of Applied Physics 117 (2015) 215304.

[51] V. Vandalon, W. M. M. Kessels, What is limiting low-temperature atomic layer deposition of Al_2O_3? A vibrational sum-frequency generation study, Applied Physics Letters 108 (2016) 011607.

[52] K. Arts, V. Vandalon, R. L. Puurunen, M. Utriainen, F. Gao, W. M. M. E. Kessels, H. C. M. Knoops, Sticking probabilities of H_2O and $Al(CH_3)_3$ during atomic layer deposition of Al_2O_3 extracted from their impact on film conformality, Journal of Vacuum Science & Technology A 37 (2019) 030908.

[53] P. S. Maydannik, T. O. Kääriäinen, D. C. Cameron, Continuous atomic layer deposition: Explanation for anomalous growth rate effects, Journal of Vacuum Science & Technology A 30 (2012) 01A122.

[54] P. Poodt, A. Illiberi, F. Roozeboom, The kinetics of low-temperature spatial atomic layer deposition of aluminum oxide, Thin Solid Films 532 (2013) 22–25. The 9th International Conference on Coatings on Glass and Plastics.

[55] P. Maydannik, T. Kääriäinen, D. Cameron, An atomic layer deposition process for moving flexible substrates, Chemical Engineering Journal 171 (2011) 345–349.

[56] J. Cai, Z. Ma, U. Wejinya, M. Zou, Y. Liu, H. Zhou, X. Meng, A revisit to atomic layer deposition of zinc oxide using diethylzinc and water as precursors, Journal of Materials Science 54 (2019) 5236–5248.

[57] B. Xia, J. Ganem, E. Briand, S. Steydli, H. Tancrez, I. Vickridge, The carbon and hydrogen contents in ALD-grown ZnO films define a narrow ALD temperature window, Vacuum 190 (2021) 110289.

[58] N. Nandakumar, B. Dielissen, D. Garcia-Alonso, Z. Liu, R. Görtzen, W. M. M. Kessels, A. G. Aberle, B. Hoex, Resistive Intrinsic ZnO Films

Deposited by Ultrafast Spatial ALD for PV Applications, IEEE Journal of Photovoltaics 5 (2015) 1462–1469.

[59] M. Vähä-Nissi, M. Pitkänen, E. Salo, E. Kenttä, A. Tanskanen, T. Sajavaara, M. Putkonen, J. Sievänen, A. Sneck, M. Rättö, M. Karppinen, A. Harlin, Antibacterial and barrier properties of oriented polymer films with ZnO thin films applied with atomic layer deposition at low temperatures, Thin Solid Films 562 (2014) 331–337.

[60] T. Weckman, K. Laasonen, Atomic layer deposition of zinc oxide: Study on the water pulse reactions from first-principles, The Journal of Physical Chemistry C 122 (2018) 7685–7694.

[61] S. Kim, S. Lee, S.-Y. Ham, D.-H. Ko, S. Shin, Z. Jin, Y.-S. Min, A kinetic study of ZnO atomic layer deposition: Effects of surface hydroxyl concentration and steric hindrance, Applied Surface Science 469 (2019) 804–810.

[62] S. F. Nelson, D. H. Levy, L. W. Tutt, M. Burberry, Cycle time effects on growth and transistor characteristics of spatial atomic layer deposition of zinc oxide, Journal of Vacuum Science & Technology A 30 (2012) 01A154.

[63] E. B. Yousfi, J. Fouache, D. Lincot, Study of atomic layer epitaxy of zinc oxide by in-situ quartz crystal microgravimetry, Applied Surface Science 153 (2000) 223–234.

[64] K. Sharma, D. Routkevitch, N. Varaksa, S. M. George, Spatial atomic layer deposition on flexible porous substrates: ZnO on anodic aluminum oxide films and Al_2O_3 on Li ion battery electrodes, Journal of Vacuum Science & Technology A 34 (2016) 01A146.

[65] H. K. Park, B. S. Yang, S. Park, M. S. Kim, J. C. Shin, J. Heo, Purge-time-dependent growth of ZnO thin films by atomic layer deposition, Journal of Alloys and Compounds 605 (2014) 124 – 130.

[66] D. Pan, T.-C. Jen, C. Yuan, Effects of gap size, temperature and pumping pressure on the fluid dynamics and chemical kinetics of in-line spatial atomic layer deposition of Al_2O_3, International Journal of Heat and Mass Transfer 96 (2016) 189–198.

[67] H. Wang, Z. Wang, X. Xu, Y. Liu, C. Chen, P. Chen, W. Hu, Y. Duan, Multiple short pulse process for low-temperature atomic layer deposition and its transient steric hindrance, Applied Physics Letters 114 (2019) 201902.

[68] T. Muneshwar, K. Cadien, AxBAxB... pulsed atomic layer deposition: Numerical growth model and experiments, Journal of Applied Physics 119 (2016) 085306.

[69] E. Guziewicz, T. A. Krajewski, E. Przezdziecka, K. P. Korona, N. Czechowski, L. Klopotowski, P. Terziyska, Zinc Oxide Grown by Atomic Layer Deposition: From Heavily n-Type to p-Type Material, physica status solidi (b) 257 (2020) 1900472.

[70] B. A. Sperling, B. Kalanyan, J. E. Maslar, Atomic Layer Deposition of Al_2O_3 Using Trimethylaluminum and H_2O: The Kinetics of the H_2O Half-Cycle, The Journal of Physical Chemistry C 124 (2020) 3410–3420.

[71] A. Werbrouck, M. Shirazi, F. Mattelaer, S. D. Elliott, J. Dendooven, C. Detavernier, A secondary reaction pathway for the alumina atomic layer deposition process with trimethylaluminum and water, revealed by full-range, time-resolved in situ mass spectrometry, The Journal of Physical Chemistry C 124 (2020) 26443–26454.

[72] A. J. M. Mackus, C. MacIsaac, W.-H. Kim, S. F. Bent, Incomplete elimination of precursor ligands during atomic layer deposition of zinc-oxide, tin-oxide, and zinc-tin-oxide, The Journal of Chemical Physics 146 (2017) 052802.

[73] H. H. Sønsteby, A. Yanguas-Gil, J. W. Elam, Consistency and Reproducibility in Atomic Layer Deposition, Journal of Vacuum Science & Technology A 38 (2020) 020804.

[74] E. Przezdziecka, E. Guziewicz, D. Jarosz, D. Snigurenko, A. Sulich, P. Sybilski, R. Jakiela, W. Paszkowicz, Influence of oxygen-rich and zinc-rich conditions on donor and acceptor states and conductivity mechanism of ZnO films grown by ALD—Experimental studies, Journal of Applied Physics 127 (2020) 075104.

[75] A. C. Kozen, M. A. Schroeder, K. D. Osborn, C. J. Lobb, G. W. Rubloff, Examining the role of hydrogen in the electrical performance of in situ fabricated metal-insulator-metal trilayers using an atomic layer deposited Al_2O_3 dielectric, Applied Physics Letters 102 (2013) 173501.

[76] S. E. Potts, G. Dingemans, C. Lachaud, W. M. M. Kessels, Plasma-enhanced and thermal atomic layer deposition of Al_2O_3 using dimethylaluminum isopropoxide, $[Al(CH_3)_2(\mu\text{-}O^iPr)]_2$, as an alternative aluminum precursor, Journal of Vacuum Science & Technology A 30 (2012) 021505.